

On the Use of Natural and Forced Convection Correlations in Predictive CFD Simulations of Liquid Pool Fires

Article in *Fire Safety Journal*, Available online 10 February 2023, 103765

This is an Accepted Manuscript.

DOI: <https://doi.org/10.1016/j.firesaf.2023.103765>

©2023. This manuscript version is made available under the CC-BY-NC-ND 4.0 license <https://creativecommons.org/licenses/by-nc-nd/4.0/>

On the Use of Natural and Forced Convection Correlations in Predictive CFD Simulations of Liquid Pool Fires

Hong M. C.^{1*}, Merci B.¹, Beji T.¹

¹ Ghent University, Dept. of Structural Engineering and Building Materials, Ghent, Belgium.

*Corresponding author's email: mingcian.hong@ugent.be

ABSTRACT

This paper presents a detailed analysis of predictive numerical simulations of liquid pool fires, i.e., a 1 m – diameter methanol pool, a 0.7 m × 0.8 m ethanol pool, and a 0.18 m – diameter heptane pool. The burning rate is predicted using the ‘film’ model, including empirical correlations for heat and mass transfer. Although the forced convection approach (used in Fire Dynamics Simulator, FDS 6.7.5) yields relatively good results in fuel evaporation rate, it is somewhat questionable from a fundamental standpoint for quiescent burning conditions. Therefore, the natural convection approach is implemented in FDS 6.7.5. The predicted burning rates are similar to the forced convection approach, but the fuel surface temperature is closer to the boiling point by the natural convection approach. Based on the extensive analysis for the methanol pool fire, a modified natural convection correlation is proposed. The latter is tested for the ethanol test with satisfactory results for the peak Heat Release Rate (HRR), burning time, and surface temperature (closer to the boiling point). The modified natural convection approach is further tested for the heptane pool fire. Improved predictions are obtained for the peak burning rate, the transient stage, and the surface temperature.

KEYWORDS: Liquid pool fires, CFD, forced convection, natural convection.

1. INTRODUCTION

Liquid pool fires are driven by a very complex interaction between several physical and chemical phenomena that occur at the level of both the gas and the liquid phase. Despite the strong advances in combustion and fire science, there are currently no fully predictive and reliable models of liquid pool fires, partly due to the strong coupling at the liquid – gas interface.

The most common approach to estimate the burning rate of a liquid pool fire and the subsequent hazards (e.g., the thermal radiation to the surroundings) is to use semi-empirical correlations such as the correlation of Babrauskas [2], where the liquid phase is fully decoupled from the gas phase, i.e., no dependence of the burning rate (and thus, the evaporation rate) on the heat flux at the liquid surface and vice versa. In the empirical correlation developed by Ditch et al. [3], the burning rate is explicitly expressed as the ratio of the total (convective and radiative) heat flux at the surface to the heat of gasification of the liquid. The convective heat flux is taken as constant and the radiative heat flux is a function of the soot yield, the burner diameter and the heat of gasification. A more advanced global model has been developed by Hamins et al. [4] where ‘the mass flux of burning fuel [...] depends on the heat feedback from the flame to the fuel surface’. All the correlations and models described above [2 – 4] have been assessed for steady-state liquid pool fires in open atmosphere and under quiescent conditions, which are rather ‘idealized’ conditions that do not represent some specific practical scenarios such as under-ventilated enclosure fires. Nevertheless, the under-ventilated enclosure fires can still be addressed with the correlation of Peatross and Beyler [5] to account for the reduction of the burning rate as a function of the oxygen concentration. However, relying on a more advanced technique such as Computational Fluid Dynamics (CFD) is an interesting alternative, given the potential to solve accurately the fire driven flow (at the level of the gas phase) and the interaction with the liquid phase.

Most of the CFD model developments have been focused so far on the gas phase (e.g., turbulence and combustion modelling) and relatively less effort has been devoted to the coupling with the liquid phase. In [6], a predictive iterative algorithm has been proposed with the aim to ‘maintain an equilibrium fuel vapor pressure in the first gas-phase cell above the liquid boundary’. The main drawback of this approach is the high sensitivity to the spatial resolution. In [7], the burning rate in a mechanically ventilated enclosure is predicted based on the heat flux at the liquid surface (divided by the heat of gasification) and the local oxygen concentration (using the correlation of Peatross and Beyler [5]) in the ‘vicinity of the flame’. One of the drawbacks of such approach is the difficulty to define the ‘vicinity of the flame’ [8], from a CFD perspective.

Currently, the most ‘popular’ approach to predict the burning rate of a pool fire using CFD is based on the so-called ‘film model’ where the local fuel evaporation rate is ‘governed by Stefan diffusion’ [6]. Two key quantities in this approach are the Sherwood number, Sh , and the length scale, L . The former is a non-dimensional number that represents the ratio of convective mass transfer to the rate of diffusive mass transport. The latter is used to estimate Sh and the so-called mass transfer coefficient, h_m . The Sherwood number is typically estimated from empirical correlations derived from steady-state parallel flow across a flat plate, assuming an analogy (i.e., the Chilton-Colburn analogy) between heat and mass transfer. Thus, the Sherwood number is taken as equal to the Nusselt number, Nu , which is estimated in the heat transfer experiments. It is important to state that the empirical correlations referred to above have not been developed for reactive flows such as pool fires. Therefore, they might not be suitable for these types of flows. It is in this context that this paper seeks to provide an in-depth analysis of the ‘film’ modelling approach for liquid fuel evaporation in CFD simulations. Neither the Chilton-Colburn analogy nor the use of the ‘empirical heat transfer correlations’ will be challenged in this paper. The focus will be rather put on the question of which correlations to use: natural or forced convection and for which regime: laminar or turbulent. In this context, an empirical correlation is used to estimate the convective mass transfer coefficient. More specifically, in [6], the choice has been to use the correlation for forced convection in the turbulent regime, which remains the option used in the Fire Dynamics Simulator (FDS 6.7.5) [9]. It has been argued in [10], based on a simplified in-house model (without solving the flow field), that the correlation for natural convection in the laminar regime might be more appropriate. We elaborate this work further by implementing the natural convection correlations in FDS 6.7.5 and assessing the CFD predictions against available data for a 1 m-diameter methanol pool fire [13] and 0.70 m \times 0.81 m ethanol pool fire [14], as discussed in the preceding paper [1]. In this paper, the study is extended to a very different fuel type and pool size, an 18 cm-diameter heptane pool fire [15]. The discussion will be not only based on the predicted burning rate(s), but also on important ‘intermediate’ variables related to the flow regime (i.e., laminar or turbulent), and the influence to the fire development. In the remainder of the paper, we will provide first a description of the main models and correlations (for heat and mass transfer) of interest in this work. Then, we will recall briefly the modelling approach used in FDS for turbulence, combustion and thermal radiation. This will be followed by a description of the experiments of interest and the numerical test cases that were carried out. Finally, a detailed discussion of the results will be undertaken, followed by the main conclusions and some elements of future work.

2. HEAT AND MASS TRANSFER MODELLING

The general modelling framework used in this work is based on the description provided in [6] and [9]. In the following section, we will recall the main elements given therein as well as the new features implemented in FDS in the context of this work, i.e., the natural convection approach.

2.1 Liquid Evaporation Model

The local evaporation rate of the liquid fuel is governed by Stefan diffusion [6]:

$$\dot{m}'' = h_m \frac{\bar{p}_m MW_F}{RT_g} \ln \left(\frac{X_{F,g} - 1}{X_{F,\ell} - 1} \right) \quad (1)$$

where h_m is the mass transfer coefficient, \bar{p}_m is the background pressure of the m^{th} pressure zone (see [9] for more details), MW_F is the molecular weight of the fuel gas, R is the universal gas constant, T_g and $X_{F,g}$ are respectively the gas temperature and the volume fraction of fuel vapor in the center of the first gas phase cell above the liquid, and $X_{F,\ell}$ is the volume fraction of the liquid vapor at the surface. The latter is calculated using the integrated Clausius–Clapeyron equation [9]:

$$X_{F,\ell} = \exp \left[-\frac{L_v MW_F}{R} \left(\frac{1}{T_s} - \frac{1}{T_b} \right) \right] \quad (2)$$

where L_v is the heat of vaporization, T_s is the surface temperature of the fuel, and T_b is the boiling temperature of the fuel. The Clausius–Clapeyron equation assumes that the specific volume of liquid phase is negligible compared to that of the gas phase and the gases behave as ideal gases [16]. The suitability of the Clausius–Clapeyron equation for a liquid–gas phase transition under combustion condition is yet to be confirmed. Some semi-empirical alternatives, such as Antoine equation [17], might generate a closer approximation for the temperature dependency of the vapor pressure (and thus $X_{F,\ell}$). Nevertheless, the use of the integrated Clausius–Clapeyron equation does not affect the main discussions in this study, i.e., the mass and heat transfer calculations based on forced or natural convection correlations (see section 2.3). Therefore, the use of Eq. (2) is not challenged here.

The mass transfer coefficient h_m is defined as:

$$h_m = \frac{\text{Sh } D_{\ell,g}}{L} \quad (3)$$

where Sh is the Sherwood number, $D_{\ell,g}$ is the diffusivity of the liquid species in the gas phase, and L is the length scale of the liquid surface, which is also used for the convective heat transfer calculations.

The key questions that open up at this stage (and which are thoroughly examined in this paper) are how to calculate Sh and L in Eq. (3), in order to calculate h_m . This will be addressed in section 2.3. But first, we will give an overview of the heat transfer modelling in which the approach to calculate the convective heat transfer coefficient, h , is analogous to the calculations of h_m .

2.2 Heat Transfer Within the Fuel

The liquid fuel is treated as a thermally thick solid, i.e., the convective motion within the solid is not directly solved. One-dimensional heat transfer is considered. Fourier's equation in the following form is solved:

$$\rho_\ell c_\ell \frac{\partial T_\ell(x,t)}{\partial t} = \frac{\partial}{\partial x} \left(k_\ell \frac{\partial T_\ell(x,t)}{\partial x} \right) + \dot{q}_r'' \quad (4)$$

where t is the time, x is the distance from the liquid surface, ρ_ℓ , c_ℓ , and k_ℓ are the density, specific heat, and thermal conductivity of the fuel and \dot{q}_r'' is the radiative exchange term (see [6] for more details).

The thermal boundary condition on the liquid surface reads:

$$-k_\ell \frac{\partial T_\ell}{\partial x}(0,t) = \dot{q}_c'' + \dot{q}_r'' - L_v \dot{m}'' \quad (5)$$

where \dot{q}_c'' is the convective heat flux and \dot{q}_r'' is the radiative heat flux. The convective heat flux at the liquid surface is calculated as:

$$\dot{q}_c'' = h(T_g - T_s) \quad (6)$$

The convective heat transfer coefficient, h , is calculated similarly to Eq. (3) as:

$$h = \frac{\text{Nu } k_g}{L} \quad (7)$$

where k_g is the thermal conductivity of the surrounding gas and Nu is the Nusselt number.

2.3 Correlations for Sh and Nu and the length scale L

2.3.1 Forced Convection Approach

The empirical correlations for the Sherwood number in the case of a flow parallel to a flat plate, and considering the Chilton-Colburn analogy (i.e., $\text{Sh} = \text{Nu}$), read [11]:

$$\text{Sh} = 0.664 \text{Re}^{1/2} \text{Sc}^{1/3} \quad \text{if} \quad \text{Re} < 3 \times 10^5 \quad (8a)$$

$$\text{Sh} = 0.037 \text{Re}^{4/5} \text{Sc}^{1/3} \quad \text{if} \quad 3 \times 10^5 < \text{Re} < 10^8 \quad (8b)$$

where Re is the Reynolds number and Sc is the Schmidt number (taken here as $\text{Sc} = 0.6$). Equations (8a) and (8b) correspond to a laminar and a turbulent regime, respectively. The Reynolds number is calculated as:

$$\text{Re} = \frac{\rho_g u L}{\mu_g} \quad (9)$$

where ρ_g and μ_g are the density and the dynamic viscosity of gas at the arithmetic mean (film) temperature of the thermal boundary layer between the surface and the surrounding gas [11], u is the velocity of the cross flow and L is the length of the plate across which the flow is developing.

It is important to recall here that our fire scenario of interest is a pool fire in open atmosphere and under quiescent conditions. Therefore, in the absence of any cross flow (e.g., induced by a wind) at the edge of the liquid pool, a fundamentally different definition of the velocity, u , is made. It is taken in [6] as the flow velocity in the gas phase cell adjacent to the liquid surface. Furthermore, the initial condition for the velocity in Eq. (9) is $u = 0$ m/s. If there is an artificial background noise, Eq. (9) will yield a very low Re. In fact, theoretically speaking, the Sherwood number must be higher than 1 and thus, Eq. (8a) gives a minimum Reynolds number, $\text{Re}_{\min} = 76$. The approach adopted in [6] consists of setting $\text{Re}_{\min} = 5 \times 10^5$ in Eq. (9) and using Eq. (8b) for the turbulent regime, which corresponds to $\text{Sh} = 1031$ and a minimum evaporation mass flux. The implications of this approach on the transient profile of the burning rate will be discussed later in the paper.

The empirical correlations for the Nusselt number for respectively the laminar and the turbulent regime read [11]:

$$\text{Nu} = 0.664 \text{Re}^{1/2} \text{Pr}^{1/3} \quad \text{if} \quad \text{Re} < 3 \times 10^5 \quad (10a)$$

$$\text{Nu} = 0.037 \text{Re}^{4/5} \text{Pr}^{1/3} \quad \text{if} \quad 3 \times 10^5 < \text{Re} < 10^8 \quad (10b)$$

where Pr is the Prandtl number (taken here as $\text{Pr} = 0.7$).

2.3.2 Natural Convection Approach

As discussed in the previous section, the forced convection configuration may not be representative of a liquid pool fire in a quiescent environment, primarily because there is no forced flow parallel to the liquid surface. Rather, it is believed that the flow at the gas-liquid interface is driven by the combustion-generated buoyancy. Therefore, instead of using a Reynolds number, it is suggested to rely on the local Grashof number, Gr , which takes into account the buoyancy force and is defined as:

$$Gr = \frac{g L^3}{\nu_{air}^2} \frac{|\rho_{air} - \rho_g|}{\rho_g} \quad (11)$$

where g is the gravitational acceleration, ν_{air} and ρ_{air} are respectively the kinematic viscosity and density of the surrounding gas (taken here as air at 20°C and thus $\nu_{air} = 1.53 \times 10^{-5} \text{ m}^2/\text{s}$ and $\rho_{air} = 1.20 \text{ kg/m}^3$) and ρ_g is the gas density in the gas phase cell adjacent to the liquid surface. The length scale L for natural convection over a plate is taken as [11]:

$$L = A / P \quad (12)$$

where A and P are respectively the area and the perimeter of the plate (assumed to be equivalent to the liquid surface in pool fires).

The empirical correlations for the Nusselt number for respectively the laminar and the turbulent regime in the natural convection correlation read [11]:

$$Nu = 0.54 (Gr.Pr)^{1/4} \quad \text{if} \quad 10^4 < Gr.Pr < 10^7 \quad (13a)$$

$$Nu = 0.15 (Gr.Pr)^{1/3} \quad \text{if} \quad 10^7 < Gr.Pr < 10^{11} \quad (13b)$$

For the sake of completeness, it is noted that in FDS 6.7.5, h is calculated as [9]:

$$h = \max \left[C |T_g - T_s|^{1/3}, \frac{Nu k}{L} \right] \quad (14)$$

where C is the coefficient of empirical natural convection models (taken $C = 1.52$ for a horizontal planar surface). Given that Nu is calculated in FDS using the forced convection expression, Eq. (14) becomes somewhat inconsistent because the first expression therein is based on natural convection whereas the second one is based on forced convection. Nevertheless, for the cases at hand in this paper, it is found that the first expression is not used in the calculations.

By analogy to Eqs. (13), the expressions for the Sherwood number read:

$$Sh = 0.54 (Gr.Sc)^{1/4} \quad \text{if} \quad 10^4 < Gr.Sc < 10^7 \quad (15a)$$

$$Sh = 0.15 (Gr.Sc)^{1/3} \quad \text{if} \quad 10^7 < Gr.Sc < 10^{11} \quad (15b)$$

where Sc is the Schmidt number (taken here as $Sc = Pr = 0.7$).

It is quite interesting to note at this stage that considering the cubic dependence of the Gr on the length scale L (see Eq. (11)) in conjunction with Eq. (15b) for natural convection in the turbulent regime, the Sherwood number, Sh , is directly proportional to L . Consequently, the mass transfer coefficient, h_m , becomes independent of the L (see Eq. (3)) and so is then the liquid evaporation rate (see Eq. (1)). This observation renders Eq. (15b) particularly attractive for CFD simulations of liquid pool fires, where the calculations are performed on a ‘cell basis’ and thus, as pointed out in [6], it is typically not very appropriate to rely on a global geometrical parameter such as L . We note that the forced convection correlation in the turbulent regime, Eq. (8b), used in [6] yields $\dot{m}'' \sim L^{-1/5}$ if Eq. (3) is used

or $\dot{m}'' \sim L^{-1}$ if the constant minimum Reynolds number, $Re_{min} = 5 \times 10^5$, is used. Therefore, as pointed out in [6], L becomes a model parameter rather than a true geometrical parameter.

2.4 A brief summary of the major assumptions of the correlations

A brief summary of the major assumptions of the correlations in this study is provided in this section (in addition to the overview provided in Table 2). The main focus of this study is the calculations of Sherwood number (Sh) or Nusselt number (Nu), as well as the definition of the characteristic length scale (L). The calculations of Sh or Nu is based on empirical correlations derived from a steady-state flow on a flat plate, where the Chilton-Colburn analogy applies. The major discussion is the comparison of the forced and natural convection approaches in the calculations of the mass and heat transfer coefficients, h_m and h , based on Sh and Nu. The local evaporation rate is calculated based on Stefan diffusion, where the mass flux is calculated using h_m , the volume fraction on the liquid surface ($X_{F,l}$) and the gas phase ($X_{F,g}$) cell adjacent to the liquid fuel. An integrated Clausius–Clapeyron equation is used for the calculations of $X_{F,l}$, assuming that the specific volume of gas phase is much larger than that of liquid phase, a constant latent heat, and an ideal gas behaviour. The heat transfer of the liquid phase is solved by 1-D Fourier's equation in a thermally thick solid. The liquid surface temperature is calculated based on the convective and radiative heat flux received on the fuel surface, as well as the cooling from evaporation.

3. TURBULENCE, COMBUSTION AND THERMAL RADIATION MODELLING

The default FDS settings are used in this work (see [9]), unless specified otherwise. Large Eddy Simulation (LES) is used for the treatment of turbulence, including the modified Deardorff model for the sub-grid scale viscosity. Infinitely fast chemistry is computed within the Eddy Dissipation Model (EDM) framework for turbulent combustion. The Radiative Transport Equation (RTE) is solved using the Finite Volume Method (FVM). A radiative fraction, χ_r , is prescribed for methanol and ethanol tests, in order to make sure that a minimum fraction from the heat generated by combustion is lost to the surroundings by thermal radiation. For the heptane pool tests, χ_r is calculated as finer grids are used in the calculations (more details can be found in section 4.3). It should be mentioned as well that the default number of radiation angles has been increased from 100 to 500 as suggested in [12].

4. EXPERIMENTAL CONFIGURATIONS AND NUMERICAL SETTINGS AND TESTS

4.1 Large – scale methanol pool fire

4.1.1 Experimental settings

The first experimental study considered in this work [13] consists of ‘a series of measurements [...] to characterize the structure of a 1 m diameter methanol (CH_3OH) pool fire steadily burning with a constant lip height in a quiescent environment’. The burner (which was water-cooled at its bottom) is a circular steel pan with an inner diameter of 1.00 m, a depth of 0.15 m, and a wall thickness of 1.6 mm. The lip height is maintained at 10 mm and the burner is mounted on cinder blocks, 0.3 m above the floor. The measured steady-state burning rate is 12.8 ± 0.9 g/s, which corresponds to a burning rate per unit area of 16.3 ± 1.2 g/m²/s. Gas phase temperature measurements at the axis of the fire plume and heat flux measurements in the surroundings of the flame are also provided. The radiative heat feedback to the liquid surface was found to represent 79% of the total heat feedback.

4.1.2 Numerical settings

Given that FDS solves the flow in a Cartesian system of coordinates, a square burner has been prescribed in the numerical simulations with a side length, $L_{burner} = 0.88$ m, which corresponds to an area $A_{burner} = 0.7744$ m² (1.4 % lower than the actual area). A preliminary study of heptane pool fire simulations demonstrates that the difference between a square and a round burner (set-up using the ‘stair stepping’ method) is marginal in the results (see section 4.3.2 for more information). The fuel

depth specified in the calculations is the same as in the experiments, i.e., 0.15 m. The prescribed lip height in the simulations is 1 cm.

The liquid fuel properties used in this work are displayed in Table 1. For methanol, the properties are taken from the FDS input file in GitHub [12]. For ethanol, they are taken from [6]. Soot and CO are not considered for these two liquids, given that we are dealing with alcohols.

Table 1 Liquid fuel properties.

Fuel	Methanol	Ethanol	Heptane
ρ (kg/m ³)	792	794	675
c (kJ/kg.K)	2.53	2.44	2.24
k (W/m.K)	0.20	0.17	0.14
L_v (kJ/kg)	1098.3	837	317
ΔH_c (kJ/kg)	20934	27474	43580
χ_r (-)	0.21	0.25	Calculated
T_b (°C)	64.6	78.5	98.5
Y_{CO}	NA	NA	0.010
Y_s	NA	NA	0.037

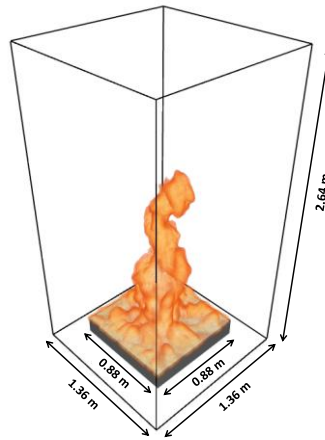


Fig. 1. A schematic view of the computational domain in the methanol pool fire tests. The six boundaries are set to ‘OPEN’.

The computational domain has been set to $1.36 \times 1.36 \times 2.64$ m³ (see Fig. 1). The height of the domain has been chosen to make sure that the flame (combustion region) does not extend beyond the top boundary. A preliminary study is conducted for the domain size, where wider ($1.92 \times 1.92 \times 2.40$ m³) and smaller ($1.20 \times 1.20 \times 2.40$ m³) domains are tested with identical numerical settings with a cell size of 8 cm. No significant difference is found for the fire history and steady state burning rate (9.18 g/s vs. 9.16 g/s for the wider domain and smaller domain, respectively). The six sides of the computational domain have been set to ‘OPEN’, which means that the fluid flow in or out of the computational domain depends on the local pressure gradient. The bottom boundary is set as ‘OPEN’ because the burner was elevated in the experiments. One test is carried out to examine the influence of the floor, e.g., change of air-entrainment or re-radiation from the floor. In this test, the burner is raised by a $0.96 \times 0.96 \times 0.30$ m³ concrete block, 0.3 m above a concrete floor. The simulation domain

is extended ($2.00 \times 2.00 \times 3.00 \text{ m}^3$) to include the floor and possible subsequent effects. The results show that the influence of the floor is marginal (around 1% difference) for the predicted burning rate.

Table 2 List of main numerical simulations.

Sim. ID	Fuel	Forced Vs. Natural ^b	Laminar Vs. Turbulent	Re_{min}	L	Cell size (cm)
FTm8	Methanol	Forced	Turbulent	5×10^5	L_{burner}	8
FTm4	Methanol	Forced	Turbulent	5×10^5	L_{burner}	4
FTm2	Methanol	Forced	Turbulent	5×10^5	L_{burner}	2
FTm1	Methanol	Forced	Turbulent	5×10^5	L_{burner}	1
FLm2 ^a	Methanol	Forced	Laminar	0	L_{burner}	2
NLm2	Methanol	Natural	Laminar	NA	A_{burner} / P_{burner}	2
NTm2	Methanol	Natural	Turbulent	NA	A_{burner} / P_{burner}	2
NTm8	Methanol	Natural	Turbulent	NA	A_{burner} / P_{burner}	8
NTm4	Methanol	Natural	Turbulent	NA	A_{burner} / P_{burner}	4
NTm1	Methanol	Natural	Turbulent	NA	A_{burner} / P_{burner}	1
NTm2_Prime ^c	Methanol	Natural	Turbulent	NA	A_{burner} / P_{burner}	2
FTe2	Ethanol	Forced	Turbulent	5×10^5	L_{burner}	2
NTe2_Prime ^c	Ethanol	Natural	Turbulent	NA	A_{burner} / P_{burner}	2
FTh4	Heptane	Forced	Turbulent	5×10^5	L_{burner}	4
FTh2	Heptane	Forced	Turbulent	5×10^5	L_{burner}	2
FTh1	Heptane	Forced	Turbulent	5×10^5	L_{burner}	1
NTh1_Prime ^c	Heptane	Natural	Turbulent	NA	A_{burner} / P_{burner}	2

^a Numerical instability occurred in this simulation before reaching the prescribed 500s simulation time.

^b $Sh = Nu = 0.664Re^{1/2}Sc^{1/3}$ is used for the laminar regime and $Sh = Nu = 0.037Re^{4/5}Sc^{1/3}$ is used for the turbulent regime, for the forced convection approach; $Sh = Nu = 0.54(Gr.Sc)^{1/4}$ is used for the laminar regime and $Sh = Nu = 0.15(Gr.Sc)^{1/3}$ is used for the turbulent regime, for the natural convection approach.

^c The correlation applied for calculations is similar to natural turbulent approach, except that the coefficient 0.15 has been lowered to 0.05, i.e., $Sh = Nu = 0.05(Gr.Sc)^{1/3}$.

The main numerical simulations carried out in this work are listed in Table 2. The nomenclature is as follows: the first letter is either F or N (Forced Vs Natural convection), the second letter is T or L (Turbulent Vs Laminar regime), the third letter is the fuel ('m' for methanol, 'e' for ethanol, and 'h' for heptane), and the number denotes the cell size in cm. The first simulations that will be analysed in this paper are based on the model choices described in [6], i.e., forced convection in the turbulent regime with $Re_{min} = 5 \times 10^5$. The first choice to be discussed here (besides the cell size, see simulations FTm8 to FTm1) is with respect to the flow regime. In other words, bearing in mind that the flow velocities at the liquid surface in case of a pool fire are typically 'low', the Re numbers are expected to be low, which would rather correspond to a laminar regime and make the choice of $Re_{min} = 5 \times 10^5$ not consistent with the actual flow conditions. Therefore, after simulations FTm8 to FTm1, FLm2 is carried out based on the implementation of Eq. (10a) (for forced convection in the laminar regime) in FDS and without setting any predefined Re_{min} .

The second series of simulations (i.e., simulations NLm2 to NTm1, see Table 2) is focused on natural convection (by implementing Eqs. (13) and (15) in FDS 6.7.5), arguing (as already discussed above) that this is more representative of the actual conditions than forced convection. The specific choice of using the turbulent instead of the laminar regime in simulations NTm2 to NTm1 is based on simulations of NLm2 and NTm2, where the Rayleigh number is found to fall in the turbulent regime. More details will be given in section 5.

It is important to bear in mind that no sensitivity analysis on the length scale L is carried out here, because the latter parameter is considered in this study as a ‘geometrical parameter’, rather than a ‘model parameter’, as advocated in [6]. Therefore, differences between the forced and natural convection approaches do not stem only from the different expressions of Sh but also from the definition of the length scale. The simulation time has been set to 500 s and the quasi-steady state parameters are averaged over the last 200 s. A moving average over 12 s is applied to the temporal profiles of the burning rate and the fuel surface temperature in order to reduce the noise of the signal. The tests for the ethanol and heptane will be discussed in the following sections.

4.2 Large – scale ethanol pool fire

4.2.1 Experimental configuration

The second test case considered in this work is a $0.70\text{ m} \times 0.81\text{ m} \times 0.05\text{ m}$ ethanol pool fire examined experimentally in [14]. The initial fuel liquid layer thickness is 9 mm and the initial lip height is about 4.1 cm. The Heat Release Rate (HRR) in open atmosphere and quiescent conditions has been measured by putting the burner under a hood.

It is important to mention at this stage that the ‘bulk’ of the numerical simulations discussed in this paper are devoted to the first test case, i.e., the 1 m – diameter methanol pool fire. By the end of this comprehensive set of simulations, we carried out one single simulation for the ethanol pool fire in order to examine the level of accuracy of the predictions without carrying out any further sensitivity analysis on numerical or physical parameters and models.

4.2.2 Numerical settings

For the ethanol pool fire tests, the computational domain is $2.40 \times 2.40 \times 3.60\text{ m}^3$ (see Fig. 2). Six sides of the boundary are set to ‘OPEN’, allowing air to flow in or out freely. The height is examined in the simulations to assure the combustion region is fully contained. The burner size is identical to the experiment and placed on a concrete floor.

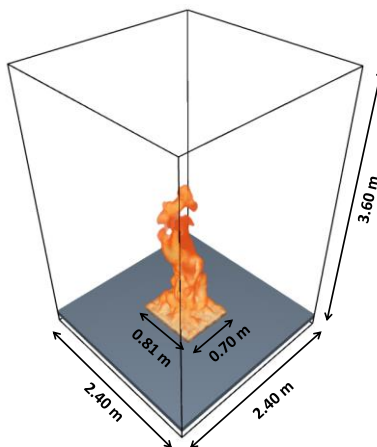


Fig. 2. A schematic view of the computational domain in the ethanol pool fire tests. The six boundaries are set to ‘OPEN’.

As mentioned earlier, the simulation settings for this test case are based on the outcome of the methanol pool fire simulations. That means that the cell size is set to 2 cm (because the pool size is similar to the methanol case). Furthermore, regarding heat and mass transfer modelling, the natural convection approach in the turbulent regime is used and compared to the forced convection approach, as described in [6]. The test cases are listed in Table 2.

4.3 Small – scale heptane pool fire

4.3.1 Experimental configuration

The third test case is an 18 cm-diameter heptane pool fires with a fuel thickness of 0.043 m, as described in [15]. The heptane pool fire is ignited by a propane burner and burns in free-burn, i.e., well-ventilated conditions. Fuel mass loss is measured by a load cell, with a measuring frequency of 1 Hz. More details of the measuring apparatus methods can be found in [15].

4.3.2 Numerical settings

A $0.16 \times 0.16 \text{ m}^2$ burner is prescribed in the numerical simulations to represent the circular burner in the experiments. The fuel depth is specified as in the experiment (0.043 m). The square burner is used due to the Cartesian system of coordinates applied in FDS. The surface area of the burner $A_{burner} = 0.0256 \text{ m}^2$, which is only 0.6 % higher than the actual burner. A preliminary numerical study is conducted between a rectangular and circular shape (by using ‘stair stepping’ method) with identical settings and mesh size (1 cm) in the calculations. The results showed that the influence of the burner shape in the results is marginal. The simulations are performed in a computational domain of $0.72 \times 0.72 \times 1.60 \text{ m}^3$ (see Fig. 3). Four sides and the top are set to ‘OPEN’, where the fluid can flow in and out freely through these boundaries without local pressure gradients. The burner is placed in the center of the domain and the bottom is the default boundary condition, where the surface temperature is maintained at the initial (ambient) temperature [9]. The fuel properties of heptane are listed in Table 1. The interest to perform this test case is to examine the capability of the modified natural convection approach (see Eqs. (16)) for a very different fuel type and burner size, compared to the methanol and ethanol tests. Heptane is much sootier than methanol and ethanol and has a higher boiling point and different fuel properties. The burner size ($0.16 \times 0.16 \text{ m}^2$) is also much smaller than the methanol ($0.88 \times 0.88 \text{ m}^2$) and ethanol ($0.70 \times 0.81 \text{ m}^2$) tests. The heptane pool fire test is also an important addition to the work discussed in [1].

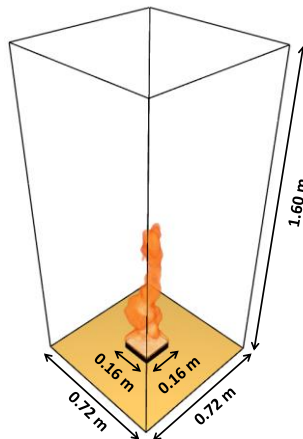


Fig. 3. A schematic view of the computational domain of the heptane pool fire tests.

The main numerical tests for the heptane pool fire are listed in Table 2. The nomenclature follows the convention described in section 4.1.2. The first set of the simulations is a cell sensitivity analysis, based on the forced turbulent approach. A preliminary study demonstrated that the default radiative fraction $\chi_r = 0.40$ in [9] yields a significantly higher MLR (1.63 g/s) than the experimental

measurement (0.46 g/s). The predicted radiative fraction approach, followed in this work, yielded a much closer MLR. It is believed that the temperature, and thus the radiative fraction, is better resolved by the finer cell (1 cm). Therefore, 1 cm is chosen as the cell size for the modified natural convection approach, and compared with the forced convection approach. The simulation time is set to 2600 s and all the fuel is consumed in the simulations.

5. RESULTS AND DISCUSSIONS

5.1 Large – scale methanol pool fire

5.1.1 Forced convection approach

Prior to the analysis of the numerical results of the first 4 simulations (see Table 2), it is believed to be of interest to perform a simplified hand calculations based on the prescribed $Re_{min} = 5 \times 10^5$ and the initial conditions for the gas, $T_g = 293$ K. By taking $Sc = 0.6$ and using Eq. (8b), one obtains a minimum Sherwood number, $Sh_{min} = 1130.91$. The binary diffusion of methanol vapor in air (using kinetic theory) is estimated as $D_{\ell,v} = 1.48 \times 10^{-5}$ m²/s. Therefore, based on the latter two values and a length scale $L_{burner} = 0.88$ m, Eq. (3) gives a mass transfer coefficient, $h_m = 0.019$ m/s. Furthermore, the initial molar concentration of methanol vapor at the liquid vapor can be taken as $X_{F,\ell} = 0.149$ by using Eq. (2) and assuming $T_s = 293$ K. The initial molar concentration of methanol vapor in the gas phase cell adjacent to the liquid is taken as $X_{F,g} = 0$. Finally, using all the above information to estimate a minimum mass loss rate per unit area (MLRPUA) based on $Re_{min} = 5 \times 10^5$ and Eq. (1) gives $\dot{m}_{min}^* \approx 4$ g/m²/s. This value is in a relatively good agreement with the value calculated by FDS after the first time step of 0.04 s and which is $\dot{m}_{min}^* \approx 5.5$ g/m²/s. Interestingly, this value appears to be in the range of critical mass flux values, i.e., 3 to 6 g/m²/s, for ignition of PMMA under various conditions as reported in [18]. Furthermore, as mentioned in [6], in order to circumvent the need to model an ignition source in the simulations, the auto-ignition temperature is set to 0 K. This allows the mixture methanol vapor – air above the liquid surface to ignite almost instantaneously at the start of the simulation, generating (thanks to the minimum MLRPUA $\dot{m}_{min}^* \approx 4$ g/m²/s) enough heat to raise continuously the surface temperature and yield a quasi-steady MLRPUA of about 22 g/m²/s when a cell size of 2 cm is used.

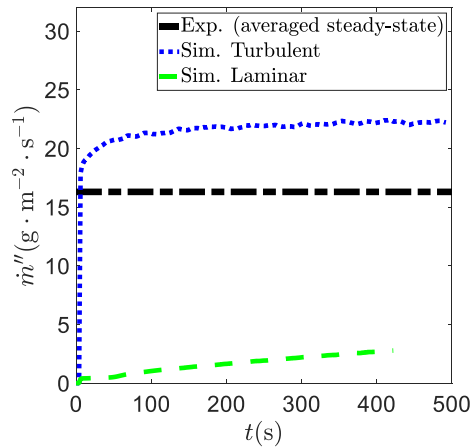


Fig. 4. Burning rate profiles for the forced convection approach with the turbulent and laminar regime, by using a 2 cm cell size.

The cell sensitivity analysis is performed and the quasi-steady state MLRPUA (averaged between 300-500 s) are displayed in Table 3. The averaged steady state burning rate is 16.3 g/m²/s in the

experiments [13]. The results show that, strictly speaking, convergence is not reached. Nevertheless, the difference between 1 cm and 2 cm simulations is sufficiently small to carry out the next simulations using the latter cell size. We note as well that from 8 cm down to 2 cm, the predicted fuel burning rate is increasing. However, the 1 cm–simulation result is slightly lower than the 2 cm–simulation result, which remains to be explained. A figure showing the fire growth of cell sensitivity analysis can be found in [1]. One numerical test is carried out to examine the influence of floor in the simulation, with the 2 cm cell size. The burner is raised 0.3 m by a concrete block from the floor. The results show that the influence of floor is insignificant on the flame structure and predicted burning rates (21.9 vs. 22.2 in g/m²/s), for the simulations with and without the floor, respectively).

Despite the physical basis behind the concept of a critical mass flux for ignition, the basis of the calculations, which is $Re_{min} = 5 \times 10^5$ is ‘questionable’. In fact, the Reynolds number, Re , in the cell adjacent to the liquid surface has been calculated in the ‘FTm2’ simulation and is found to be in the range [500 – 2500], which is two orders of magnitude lower than the prescribed $Re_{min} = 5 \times 10^5$, indicating that the flow is laminar rather than turbulent [11]. This has led us to run the simulation FLm2 (see Table 2), where the laminar regime is considered and no minimum Re is prescribed. The latter setting implies that the Reynolds number used in the calculations is solely based on the flow velocity, u , which is the result of the combustion-generated buoyancy. The profiles displayed in **Fig. 4** show that the burning becomes in this case very slow in comparison to the simulation FTm2 and no steady-state is reached within the 500 s simulation time.

Table 3 The predicted steady state MLRPUA, by the forced convection approach in the turbulent regime.

Sim. ID	FTm1	FTm2	FTm4	FTm8
\dot{m}'' (g/m ² /s)	21.0	22.2	15.8	12.5
Deviation from exp.	+28%	+36%	-3%	-23%

5.1.2 Natural convection approach

Before discussing the profiles for the natural convection approach, it is important to recall here that Eq. (11) for Gr , in conjunction with Eqs. (15), does not give a minimum Sherwood number (which would correspond to a minimum fuel mass flux), yet the burning rate in the natural convection approach increases quite rapidly. In fact, from the start of the simulation, combustion occurs (because the auto-ignition temperature has been set to 0 K) and yields a high gas temperature in the gas phase cell adjacent to the liquid. By virtue of the ideal gas law, such temperature corresponds to a relatively low gas density in the very same cell (see **Fig. 5a**), which will generate, early in the simulation, relatively high Grashof and Rayleigh (= $Gr.Pr$) numbers (see **Fig. 5b**). Based on the above results, an advantage of the natural convection approach over the forced convection approach is that the liquid evaporation rate is not dependent on the flow field at the interface liquid – gas, but only on the gas temperature (and thus density). Nevertheless, a further analysis of simulation NLm2 shows that the Rayleigh number, $Ra = Gr.Pr$, at quasi-steady state is between 2×10^8 and 3×10^8 (see **Fig. 5b**), which corresponds to a turbulent regime rather than a laminar one. That is why the simulations carried out after NLm2 were based on the correlation for the turbulent regime. On the other hand, the flow velocity above the liquid surface is found to be generally small (< 1 m/s) to sustain a Reynolds number as high as 5×10^5 (the lower bound for the turbulent regime), which is applied in the forced convection approach.

Table 4 Averaged MLRPUA in steady state predicted by the natural convection approaches.

Sim. ID	NTm2_Prime	NLm2	NTm1	NTm2	NTm4	NTm8
\dot{m}'' (g/m ² /s)	17.5	22.1	18.0	24.0	16.8	13.4
Deviation from exp.	+7%	+36%	+10%	+47%	+3%	-18%

The predicted burning rate by the laminar regime correlation is lower than the turbulent regime, as shown in Table 4. The cell size sensitivity analysis displayed in Table 4 (averaged between 300-500 s) gives qualitatively the same trend as for the forced turbulent approach. Nevertheless, the difference

between the 1 cm and the 2 cm results appears to be slightly higher. The burning rate profiles by the natural convection approach can be found in the proceeding paper [1].

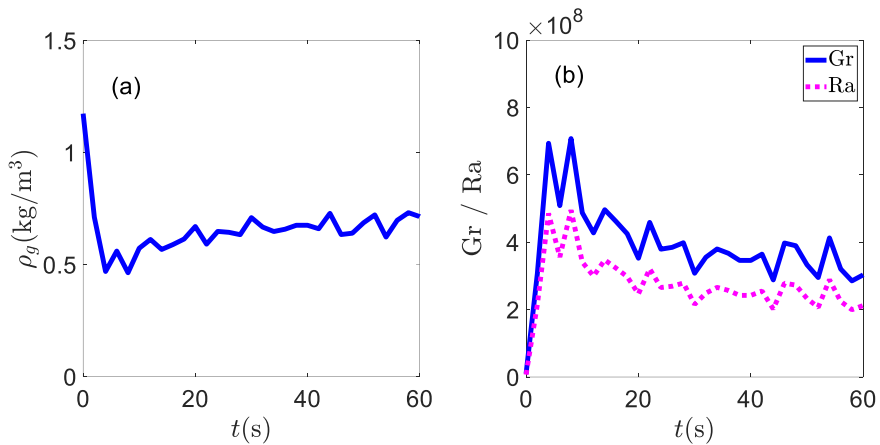


Fig. 5. Temporal profile of the (a) gas density near the liquid surface and (b) Gr and Ra for the first 60 s of simulation NL2 (see Table 2) in the center of the pool.

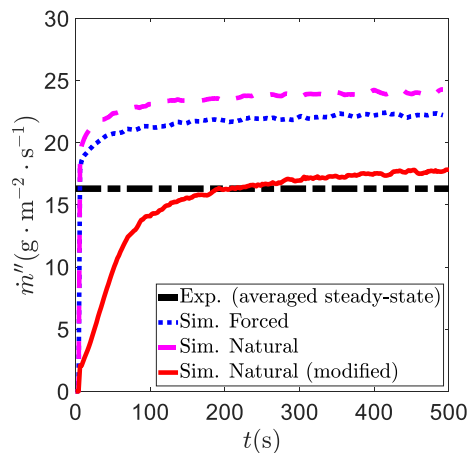


Fig. 6. Burning rate profiles using the forced, the natural and the modified natural convection approach.

Fig. 6 shows that the burning rate predictions by a forced or natural convection approach are quite similar, yielding both an overestimation of about 36% and 47 %, respectively. Besides several potential reasons linked to the gas phase, it is believed that an adjustment of coefficients used in the heat and mass transfer correlations of interest might help improving the agreement with the experimental data. One reason for modifying the coefficient is that the correlations have been developed for the scenario of a heated plate facing upward in air, rather than for pool fires. For an upward facing hot plate, the temperature on the plate surface is higher than the ambient fluid in contact with the plate. In this case, the flow is essentially upward from the plate surface, with cooler ambient fluid flowing inward over the plate surface due to natural entrainment, thereby replacing the ascending (warmer) fluid, and hence stimulating the heat transfer by sustained relatively large temperature difference between the plate surface and the fluid in contact with the surface. In the case of pool fires, the heat and mass transfer are rather dominated by the combustion-induced buoyancy. This induces air entrainment from the sides, very much like for the upward facing hot plate, but the mixture of air, fuel vapour and combustion products will have a higher temperature than the ambient air (which may even be higher than the surface temperature of the liquid fuel). This strongly affects the convective

heat transfer. Also, the heat transfer from the flame by radiation is an aspect that is not present in the situation of a heated plate in air. Equations (13) and (15) are based on a flow induced by natural convection, rather than a (strong) forced flow. Nevertheless, the flow conditions might still not be perfectly representative for the cases at hand, as the correlations have been developed for conditions without combustion. A modification of the coefficient is decided in order to improve the results. It is described in [11] that $\overline{Nu}_L = C(Gr.Pr)^n$ can be applied for many engineering calculations, where the power coefficient ‘ n ’ is 1/4 for laminar flow and 1/3 for turbulent flow. As the flow regime is found to be turbulent in the simulations, ‘ n ’ is kept as 1/3. The modification is thus carried out for the coefficient ‘ C ’ (i.e., 0.15). Several values have been tested in the range from 0.03 up to 0.15, and the value 0.05 was selected on the basis of good agreement (less than 7.1% difference) with the experimental data, for averaged MLRPUA in quasi-steady state. Although the modification remains a calibration exercise to approximate the experimental data, the new correlation is intended to be further examined for a wider range of experimental conditions, in terms of fuel type and burner diameter (see section 5.2 and 5.3). In this context, the simulation Natural (modified) in **Fig. 6** has been carried out by prescribing the same settings as NTm2, except that the coefficient 0.15 in Eqs. (13b) and (15b) has been lowered to 0.05, to account for the reduced flow effect. The proposed modified equation reads:

$$Nu = 0.05(Gr.Pr)^{1/3} \quad \text{if} \quad 10^7 < Gr.Pr < 10^{11} \quad (16a)$$

$$Sh = 0.05(Gr.Sc)^{1/3} \quad \text{if} \quad 10^7 < Gr.Sc < 10^{11} \quad (16b)$$

Table 5 Average heat fluxes at the liquid surface for the forced, natural and natural modified approaches.

Heat Flux	Forced	Natural	Natural (modified)
\dot{q}_{total}^* (kW/m ²)	24.8	27.4	20.8
\dot{q}_r^* (kW/m ²)	17.5 (71%)	16.7 (61%)	16.4 (79%)
\dot{q}_c^* (kW/m ²)	7.3 (29%)	10.7 (39%)	4.4 (21%)

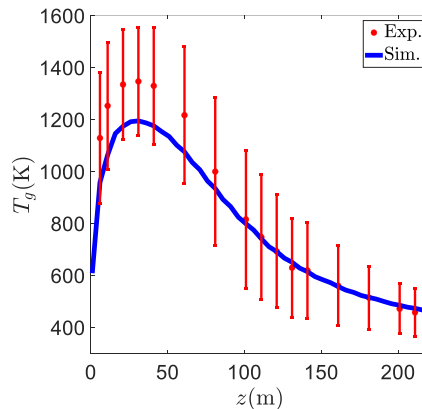


Fig. 7. The temperature predictions by the modified natural convection approach, as well as the mean and standard deviation of experimental measurements in steady state burning.

The gas temperature is well predicted by the modified correlations (i.e., Eqs. (16)), and falls within the experimental uncertainty up to about 2 m from the liquid surface, as shown in **Fig. 7**. The total heat flux values displayed in Table 5 are consistent with the predicted burning rates shown in **Fig. 6**,

where the higher the heat flux the higher the burning rate. Additionally, the modified natural approach predicted a radiative heat feedback corresponding to the experimental value (79%) [13]. In [13], the heat fluxes are measured vertically (with a radial distance of 2.07 m from the burner centreline) and horizontally (at the same height of the burner rim). The results show that the modified natural convection approach closely captures the heat flux distribution in the horizontal plane (**Fig. 8(b)**). The heat flux distribution along the vertical line is also captured but slightly under-predicted (**Fig. 8(a)**).

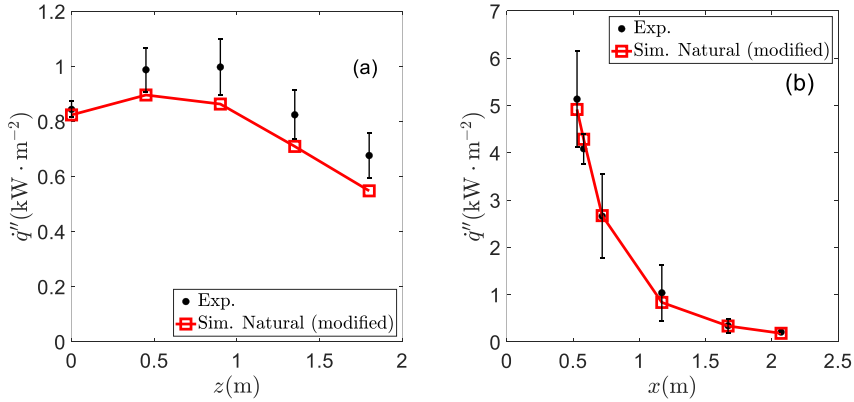


Fig. 8. The measured heat fluxes (and standard deviation) in the experiments and simulations. (a) the heat flux as a function of vertical distance above the burner rim (with a horizontal distance of 2.07 m from the burner centreline); (b) the heat fluxes as a function of horizontal distance from the burner centreline (at the same height of burner rim). Note that the domain mentioned in section 4.1.2 has been extended in order to position the heat flux gauges at the correct locations.

The results are further analysed in **Fig. 9** and **Fig. 10**, which give the radial distribution of the total heat flux and the surface temperature for simulations by the forced turbulent, natural turbulent, and modified natural turbulent convection approaches. The distributions of the total heat flux and the temperature on the liquid surface are shown in **Fig. 10**. It is observed that the surface temperature is closer to the boiling point by the natural convection approach(es). The deviations are particularly substantial near the burner wall. The results show that the predictions of the natural convection approach are closer to reality, as the fuel surface temperature is reported to be at the boiling point (65 °C) in the experiments [13]. It is observed that the flame height and flow velocity are lower by the modified natural convection approach, which is a direct consequence of the lower burning rate prediction.

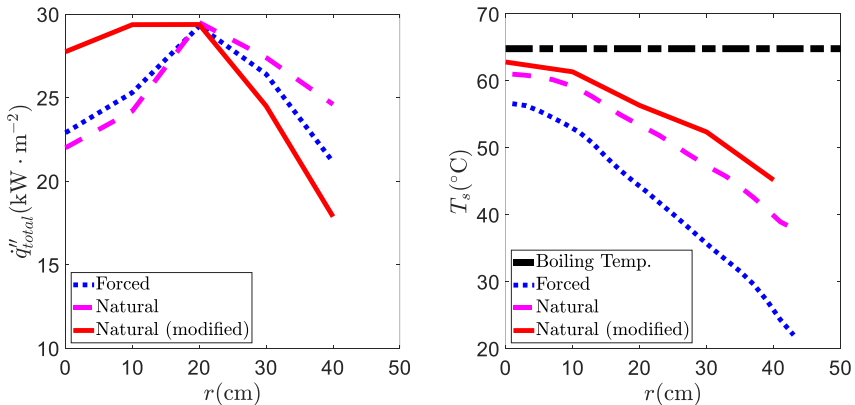


Fig. 9. Radial distribution of the total heat flux (left) and the liquid surface temperature (right) for the forced, natural and modified natural approaches.

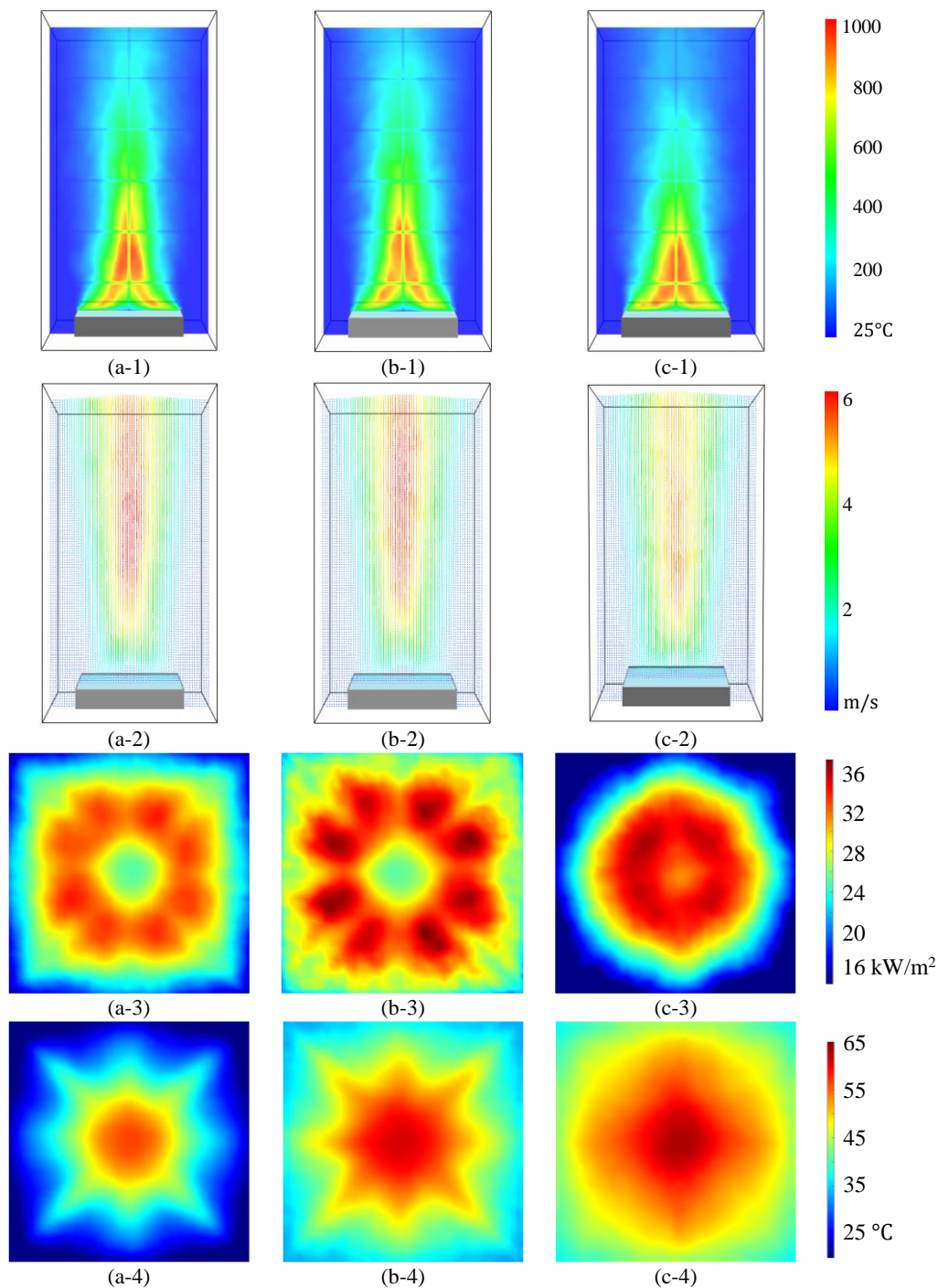


Fig. 10. The profiles of averaged (1) temperature and (2) flow velocity above the burner's center, as well as (3) total heat flux and (4) temperature on the fuel surface, during the steady state burning (averaged for 200 s). The profiles are predicted by the (a) forced, (b) natural, and (c) modified natural convection approaches.

5.2 Large – scale ethanol pool fire

Fig. 11 (left) shows that the transient behaviour of the HRR is not well captured by the simulations. However, the peak values are in a good agreement. It is noted that the modified natural approach gives

a slight improvement regarding the transient stage in that the quasi-steady stage is not reached (too) quickly as the forced convection approach. This is believed to be important in the predictions of the surface temperature displayed in **Fig. 11 (right)**. In fact, it is argued that a sudden increase in the burning (evaporation) rate, as in the forced approach, causes a substantial evaporative cooling (see the third term on the right-hand side of Eq. (5)) that prevents the liquid surface temperature from rising to sufficiently high levels. Experimental measurements are not available, but it is reported in [6] that the surface temperature reaches the boiling point in the test. The modified natural approach predicts a temperature closer to the boiling point than the forced convection approach, as shown in **Fig. 12**.

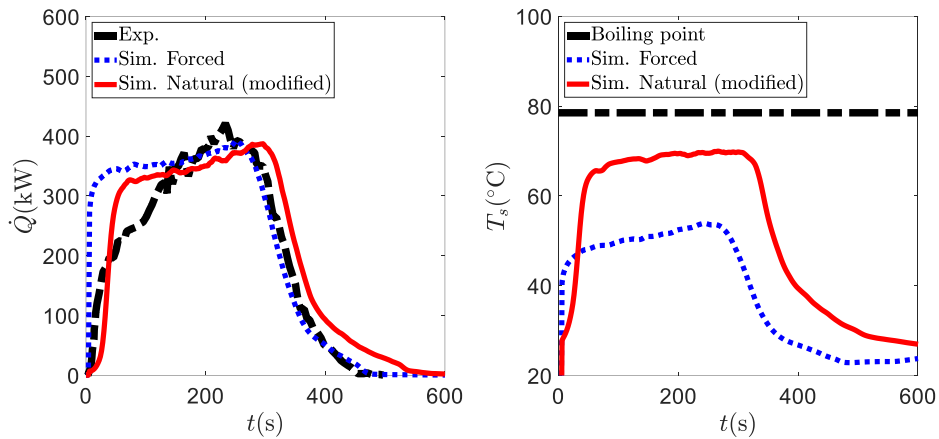


Fig. 11. Predictions of the HRR profile (left) and the evolution of the liquid surface temperature averaged across the whole surface (right) for the ethanol pool fire using the forced and the natural (modified) approach.

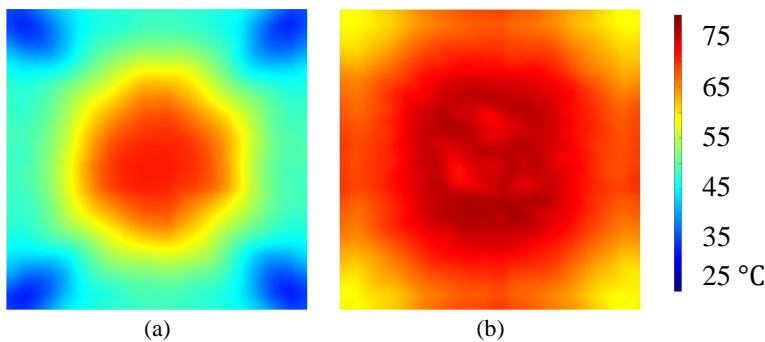


Fig. 12. The temperature profile of on the ethanol fuel surface, during the steady state burning (averaged for 100 s), by the (a) forced and (b) modified natural convection approaches.

5.3 Small – scale heptane pool fire

A preliminary study of the burner shape (square vs. circular) is conducted, as a $0.16 \times 0.16 \text{ m}^2$ square burner is used in the simulations to represent the 18 cm diameter burner in the experiments. Only marginal difference is found in the fire history and averaged steady state burning rate (0.53 g/s vs. 0.50 g/s for the square and circular burner respectively, around 4% in difference). The modified natural convection approach closely predicts the peak burning rate as well as an improved fire growth period and onset of fire decay, as shown in **Fig. 13**. Heptane is very different for certain fuel properties, such as heat of vaporization, heat of combustion, boiling point, and sootiness, compared to methanol and ethanol. Additionally, the fuel size of heptane ($0.16 \times 0.16 \text{ m}^2$) is much smaller than those of methanol ($0.88 \text{ m} \times 0.88 \text{ m}^2$) and ethanol ($0.70 \text{ m} \times 0.81 \text{ m}^2$) tests. The results show that the modified natural convection approach can fairly predict the burning rate in more general cases in terms of fuel

type and burner size. The prediction of fire history is improved by the modified natural convection approach, whereas the forced turbulent convection approach over-predicts the peak burning rate and fire growth. Moreover, as shown in **Fig. 14**, the natural convection approach also predicts a higher surface temperature, which is believed to be closer to reality. The steady state burning rates by the forced and natural convection approaches are listed in Table 6. The burning rates are averaged between 800-1000 s, except ‘FTh4’ is averaged between 500-700 s, due to faster fuel consumption in the simulation. In the experiment [15], the averaged steady state burning rate is 0.46 g/s.

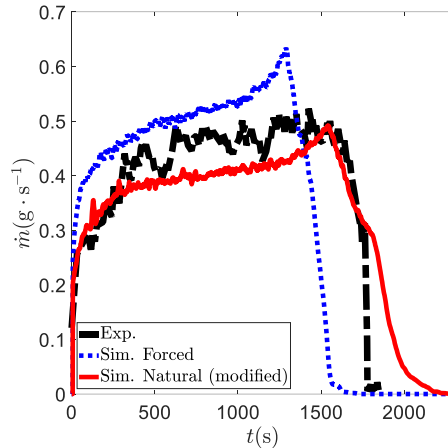


Fig. 13. The heptane pool fire burning rate in the experiment and the predictions by the forced and modified natural convection approaches.

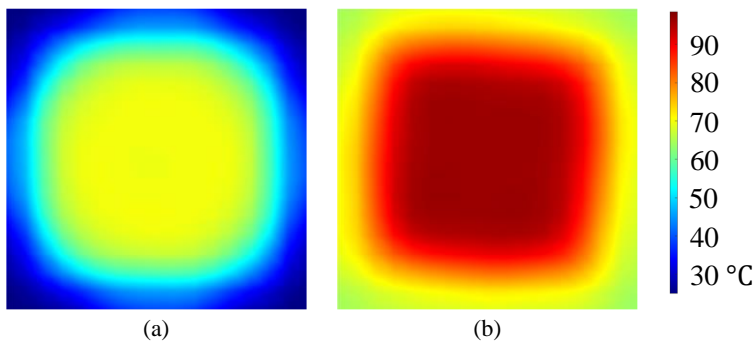


Fig. 14. The temperature profile of on the heptane fuel surface, during the steady state burning (averaged for 200 s), by the (a) forced and (b) modified natural convection approaches.

Table 6 Averaged steady state burning rate predictions by the forced and modified natural convection approaches, for the heptane pool fire test.

Sim. ID	NTh1_PRIME	FTh1	FTh2	FTh4
\dot{m} (g/s)	0.41	0.53	0.43	0.89
Deviation from exp.	-12%	+14%	-6%	+94%

6. CONCLUSIONS

In this work, natural convection correlations are implemented in the Fire Dynamics Simulator (FDS) for heat and mass transfer in predictive simulations of liquid pool fires (a 1 m – diameter methanol pool fire, a 0.7 m × 0.8 m ethanol pool fire, and a 0.18 m – diameter heptane pool fire). Based on qualitative and quantitative arguments, the natural convection approach is believed to be more relevant than the current forced convection approach in FDS, especially in the absence of a cross flow,

such as wind. Additionally, the flow regime is shown to be turbulent at the liquid–gas interface by post-processing the Rayleigh number in the natural convection approach. In terms of burning rate predictions, the deviations between the forced and the natural approaches are not significant for methanol and ethanol. However, the predicted liquid surface temperature is significantly closer to the boiling point and this is believed to be more representative of reality. An adjustment of the natural convection correlation is proposed in this paper in order to improve the predictions for the pool fires of interest. It is found that the modified natural convection approach predicts a closer burning rate to the experiments. Moreover, the results of heptane pool fire show that the modified natural convection approach can be applied in more general cases in terms of fuel type and burner size. Another aspect to be examined in future work is to consider mixed convection correlations. This allows the selection of the appropriate type of correlation to use (natural or forced and laminar or turbulent) without *a priori* knowledge of the actual conditions to be simulated, e.g., quiescent conditions or fire plume subject to a wind.

ACKNOWLEDGMENTS

This work was supported by Bel V [Scientific Research Agreement A18/TT/0674, Amendment N°1, Reference A19/TT/1632]. The authors would also like to thank the support from the FDS team, especially to Randall McDermott, Marcos Vanella, and Glenn P. Forney, for sharing their experience in modifying and compiling the source code of FDS.

REFERENCES

- [1] M. C. Hong, B. Merci, T. Beji, A Comparative Study on the Effect of Natural and Forced Convection Correlations on the CFD Simulation Results of Liquid Pool Fires, Proceedings of the 10th International Seminar on Fire and Explosion Hazards, 2022.
- [2] V. Babrauskas, Estimating large pool fire burning rates, *Fire Technology* 19 (1983) 251-261.
- [3] B.D. Ditch, J.L. de Ris, T.K. Blanchat, M. Chaos, R.G. Bill, S.B. Dorofeev, Pool fires – An empirical correlation, *Combust. Flame* 160 (2013) 2964-2974.
- [4] A. Hamins, J.C. Yang, T. Kashiwagi, A global model for predicting the burning rates of liquid pool fires, Report No. NISTIR 6383, National Institute of Standards and Technology, Gaithersburg, Maryland, USA, 1999.
- [5] M. Peatross, C. Beyler, Ventilation Effects On Compartment Fire Characterization, *Fire Safety Science* 5 (1997) 403-414.
- [6] T. Sikanen, S. Hostikka, Modeling and simulation of liquid pool fires with in-depth radiation absorption and heat transfer, *Fire Saf. J.* 80 (2016) 95-109.
- [7] S. Suard, M. Forestier, S. Vaux, Toward predictive simulations of pool fires in mechanically ventilated compartments, *Fire Saf. J.* 61 (2013) 64.
- [8] J. F. P. Segovia, T. Beji, B. Merci, CFD simulations of pool fires in a confined and ventilated enclosure using the Peatross – Beyler correlation to calculate the mass loss rate, *Fire Technology* 53 (4) (2017) 1669 – 1703.
- [9] National Institute of Standards and Technology, Gaithersburg, Maryland, USA, and VTT Technical Research Centre of Finland, Espoo, Finland. *Fire Dynamics Simulator, Technical Reference Guide*, 6th ed., March 2020. Vol.1: Mathematical Model; Vol.2: Verification Guide; Vol.3: Validation Guide; Vol.4: Configuration Management Plan.
- [10] T. Beji, B. Merci, Development of a numerical model for liquid pool evaporation, *Fire Safety Journal* 102 (2018) 48-58.
- [11] P. Incropera, D.P. de Witt, *Introduction to Heat Transfer*, Wiley, New York, United States, 1996.

- [12] FDS input file on GitHub. https://github.com/firemodels/fds/tree/master/Validation/NIST_Pool_Fires/FDS_Input_Files, (Accessed 11 June 2021)
- [13] K. Sung, J. Chen, M. Bundy, A. Hamins, The characteristics of a 1 m methanol pool fire, *Fire Safety Journal*. 120 (2020), 103121.
- [14] I. R. Thomas, K. A. M. Moinuddin, I. D. Bennetts, The effect of fuel quantity and location on small enclosure fires, *J. Fire Protect. Eng.* Vol. 17 (2007), 85–102.
- [15] M. Mense, Y. Pizzo, H. Pretrel, C. Lallemand, B. Porterie, Experimental and numerical study on low-frequency oscillating behaviour of liquid pool fires in a small-scale mechanically-ventilated compartment, *Fire Saf. J.* 108 (2019) 102824.
- [16] M. J. Moran, H. N. Shapiro, *Fundamentals of Engineering Thermodynamics* 5th Ed., Wiley, England, 2006.
- [17] G. WM. Thomson, The Antoine equation for vapor-pressure data, *Chemical Reviews*, 1946, 38, 1, 1–39.
- [18] D. J. Rasbash, D. D. Drysdale, D. Deepak, Critical Heat and Mass Transfer at Pilot Ignition and Extinction of a Material, *Fire Safety Journal* 10(1986) 1-10.